Bayesian monitoring of substructures under unknown interface assumption

Eshwar Kuncham, Neha Aswal, Subhamoy Sen, Laurent Mevel

▶ **To cite this version:**

Eshwar Kuncham, Neha Aswal, Subhamoy Sen, Laurent Mevel. Bayesian monitoring of substructures under unknown interface assumption. Mechanical Systems and Signal Processing, 2023, 193, pp.110269. 10.1016/j.ymssp.2023.110269 . hal-04148639

HAL Id: hal-04148639

https://inria.hal.science/hal-04148639

Submitted on 3 Jul 2023

HAL is a multi-disciplinary open access archive for the deposit and dissemination of scientific research documents, whether they are published or not. The documents may come from teaching and research institutions in France or abroad, or from public or private research centers.

L'archive ouverte pluridisciplinaire **HAL**, est destinée au dépôt et à la diffusion de documents scientifiques de niveau recherche, publiés ou non, émanant des établissements d'enseignement et de recherche français ou étrangers, des laboratoires publics ou privés.

Distributed under a Creative Commons Attribution 4.0 International License

Bayesian monitoring of substructures under unknown interface assumption

Eshwar Kuncham[a], Neha Aswal[a], Subhamoy Sen[a,*], Laurent Mevel[b]

[a] *i4S Laboratory, Indian Institute of Technology Mandi, Mandi, HP, India*
[b] *Univ. Gustave Eiffel, Inria, Cosys-SII, I4S, Campus de Beaulieu, Rennes, France*

Abstract

Structural Health Monitoring (SHM) enables assessing in-service structures' performance by localizing structural anomaly instances immediately after their occurrence. Typical SHM approaches monitor the entire structural spatial domain aggravating the required density and cost of instrumentation. Further, with model-based approaches, the entire structural domain is needed to be defined with high dimensional, compute-intensive models rendering the SHM approaches ill-posed and slow especially when the instrumentation is limited and system observability is compromised. Moreover, in absence of high-fidelity models, oversimplification and subsequent model inaccuracies may lead to inaccurate estimation and possibly false alarms even if a subdomain is modeled inaccurately, e.g. support boundaries. To mitigate such issues, stand-alone monitoring focusing only on a subdomain of interest may be a computationally cheaper and prompt approach while being substantially robust to false alarms. Typically, such stand-alone substructure monitoring approaches demand extensive measurement of the interface, which can be a challenge in real-life applications. This paper presents a novel filtering-based online time domain approach for estimating substructure parameters without the need to measure or estimate the substructure interfaces. The proposed component-wise estimation is stand-alone so that the health estimation of the complete structural domain can be undertaken in parallel and later coupled through post-processing. The requirement of the interface measurement has been alleviated by employing an output injection approach. The proposal has been validated on a numerical beam structure subjected to arbitrary forces and subsequently, the sensitivity against noise and damage severity of the proposal has been investigated. Finally, the proposal is validated on a real beam to illustrate its real-life applicability and significance.

Keywords: *Substructure, Random loading, Health estimation, Particle filter, Interacting filtering, Unknown interface conditions.*

1. Introduction

Structural health deteriorates over time due to crack development, water seepage, rusting reinforcements, and damage caused under extreme conditions such as earthquakes, wind storms, etc. Such deterioration

*Corresponding author; *E-mail address: subhamoy@iitmandi.ac.in*

eventually leads to their failure causing economic loss, service downtime, and in some unfortunate cases, loss of human lives. Continual monitoring of the health of the structures (termed Structural Health Monitoring (SHM)) has been traditionally adopted to avert such sudden catastrophic structural failures. Under vibration-based SHM, while frequency-based approaches have been assessed as efficient in the detection of structural deterioration, localization performance has not been proven to be well grounded. The alternative time domain methods [5, 6] have typically been associated with a predictive model in the model-assisted health assessment approach wherein the predictor model brings in the additional spatial correlation into the context. Eventually, such approaches depend on the quality of the predictive model [4, 5, 7, 23]: a simplified unrealistic model, therefore, will definitely lead to improper estimation and in some cases false alarms.

Further, due to real-life uncertainties and lack of knowledge of the ambient forcing, measurement noise recorded in the sensors, and the unavoidable model inaccuracy, deterministic approaches [4, 27] for real-life SHM can only be simplistic in nature and can rarely conform to the reality. Eventually, in this context, Bayesian filtering-based approaches have gained popularity [2, 33] addressing such uncertainties in a more systematic manner. A recursive Bayesian framework defines the problem in state-space [2] wherein structural health can be parameterized and estimated as additional states. The state evolution is generally defined using a predictive model (usually a high-fidelity Finite Element Model(FEM)) for the structural domain of interest defined in the probabilistic domain (as process model) powered by a Chapman-Kolomogorov formulation. The relationship between states and measurements is further defined using a measurement model, which takes the measurement uncertainty into consideration. The recursive formulation further estimates the states drawing inference from the departure between the model-predicted and actual response.

The Kalman filter (KF) [19], being a linear filter, is capable of solving linear state estimation problems. Yet, for SHM, models are inherently nonlinear since the states and parameters are either estimated using a bi-linear formulation with health parameters being the additional states or the states are observed through a nonlinear measurement model (typically high-fidelity FEM) [3]. This entails the employment of nonlinear and approximate filters, such as Extended (EKF) [9], Unscented (UKF) [13, 21], Ensemble (EnKF) [15] Kalman filters or Particle filter (PF) [8] for such estimation problems. While PF is considered to be a robust approach for solving nonlinear problems, the concerns related to its high computational demand led to the advent of interacting filtering techniques [14, 25, 26, 37] wherein the parameters are estimated through an interactive strategy reducing the overall state dimension [24, 37]. Herein, the parameters are estimated using PF while KF/EnKF has been employed for state estimation depending on the nature of the process model (linear or nonlinear).

Improved SHM techniques, capable of addressing uncertainties, nonlinearity, etc. may however falter due to the increased dimensionality of the prediction model when dealing with very large structures. Along with the increased computational cost of SHM, high dimensionality often leads to several false positive alarms. For the model-assisted estimation approach, consequent high-resolution monitoring of the real structure

requires extensive instrumentation. With limited measurement channels (usual for any SHM application), employment of high dimensional models affects the observability [20]. This eventually renders the SHM algorithm to be inefficient and unreliable. An effective way of monitoring large structures is to monitor one subdomain at a time instead of monitoring the entire structure at once. Numerically decoupling a structure into smaller substructures for efficient analysis of the structure is known as substructuring. Large complex structures can be economically monitored with the help of the substructuring techniques [18] as it reduces the required resources as well as the need for measurement data from inaccessible locations.

With the aim of model reduction [16], substructuring can be done in the physical (mass, stiffness, etc.), frequency (Fourier transform), or modal (eigenvalue decomposition) domain. Nevertheless, the substructures have been predominantly defined in modal domain [11, 12, 38] with a few exceptions [17] where they are defined in the time domain. Numerical substructuring does not physically isolate a subdomain from the rest, but only fragments the entire domain numerically into smaller manageable domains. Eventually, these fragmented subdomains individually should conform to the force equilibrium or displacement continuity. The interaction among them is generally incorporated in terms of the interface forces between the substructures [30]. These interface forces can later be estimated during the re-coupling of the component substructures in order to realize the original entire structure [16].

Nonetheless, the external force inputs are hardly known/measured in real-life problems, either explicitly or statistically. Such forces can however be estimated as additional states [10, 28, 29] which will eventually increase the state dimension and consequently, the complexity and efficiency of the state estimation. Moreover, health state assessment for a structure is also sensitive to changes in internal forces (prestress) as well as boundary conditions [22]. Boundary forces, present on the substructural boundary degrees of freedom (DoFs), have also been directly measured [32] as well as estimated by modeling them as modulated filtered white noise [35] or by constructing a relationship between the interface forces and the measured responses [34]. Forward genetic algorithms have been utilized to directly use the interface measurement data (sensor output) to account for the interface interaction instead of estimating interface force [17, 31]. Not only do these aforementioned algorithms require extensive monitoring of all the interfaces, which are generally not accessible in real structures, but also they make all the substructure models interdependent.

With an objective to develop a component-wise monitoring algorithm, [36] introduced a probabilistic frequency domain approach wherein Bayesian inference has been employed to monitor only a subdomain of interest. In this article, the substructures to be monitored have been categorized as either stable (supported subdomain with defined Dirichlet boundary condition without any rigid motion), or unstable (unsupported subdomain equilibrated with interface forces and subjected to rigid motion). The approach was further numerically investigated in a multi-story building to estimate the parameters using recorded substructure response under certain driving forces (a single channel base excitation and a force generated by a vibrating machine). Even though both the substructure types (stable and unstable) are discussed, the numerical

experimentation has been taken up only for the stable substructures, and thereby the importance of modeling the rigid motion of the unstable substructures has been missed. Further being defined in the frequency domain, the approach is not an online algorithm that can be implemented in real-time.

The present study proposes a novel computationally efficient online structural health assessment approach that bypasses the requirement of the interface force quantities and is also applicable for stand-alone stable as well as unstable substructures. The numerical and experimental studies have been performed on unstable substructures where substructural boundaries are set as unknown/free. The proposed approach utilizes output injection methodology [24, 39] in order to be robust to variations in the interface force/acceleration with the help of known measurement data of the internal nodes of the particular substructure. This makes targeted health monitoring of the substructure possible, without the need of monitoring the other substructures. An interacting filtering strategy combining PF and EnKF (IPEnKF), for the estimation of health parameters and states respectively, has been utilized in this attempt. Complexity in system estimation depends majorly on observability issues (generally originating from lack of instrumentation) rather than the physical size or geometric complexity of the system. Accordingly, both numerical and experimental validations of the proposed algorithm have been undertaken on a minimally instrumented simply supported beam. Further, noise sensitivity, limiting damage severity, and required sensor density to assess the scalability of the algorithm have also been investigated for the proposed approach. The need for information on boundary conditions for SHM of a structure can also be bypassed with the proposed algorithm, which has been demonstrated later in this article with numerical and experimental studies.

2. Robust state-space formulation for substructure system

For Bayesian filter-based SHM algorithms, the structural dynamics have to be defined in state-space form. The governing differential equation (GDE) detailing the linear time-varying dynamics for the entire structural domain, $\mathbf{\Omega}$, can be defined with time-invariant mass $\mathbf{M}$, time-varying stiffness $\mathbf{K}$(t), damping $\mathbf{C}(t)$ matrices, and external force $\mathbf{f}$(t) as,

$$\mathbf{M}\ddot{\mathbf{q}}(t) + \mathbf{C}(t)\dot{\mathbf{q}}(t) + \mathbf{K}(t)\mathbf{q}(t) = \mathbf{f}(t) \tag{1}$$

where $\mathbf{q}(t)$, $\dot{\mathbf{q}}(t)$, and $\ddot{\mathbf{q}}(t)$ are the displacement, velocity, and acceleration response at the nodes.

2.1. Substructural dynamics

The overall system domain $\mathbf{\Omega}$ can further be divided into N_s independent non-overlapping substructures $\mathbf{\Omega}^s$, where $s = 1, 2, \ldots, N_s$. Each substructure can further be defined with two domains: internal, $\mathbf{\Omega}^{s_i}$, and interface boundary, $\mathbf{\Omega}^{s_b}$. Except for the nodes lying on $\mathbf{\Omega}^{s_b}$, all the nodes of the component substructures belong exactly to one substructure. Accordingly, the GDE for $\mathbf{\Omega}^s$ can be decoupled from that of $\mathbf{\Omega}$ by compensating with the unmeasured interface forces $\mathbf{g}_b^s(t)$.

$$\begin{bmatrix} \mathbf{M}^s_{ii} & \mathbf{M}^s_{ib} \\ \mathbf{M}^s_{bi} & \mathbf{M}^s_{bb} \end{bmatrix} \begin{Bmatrix} \ddot{\mathbf{q}}^s_i \\ \ddot{\mathbf{q}}^s_b \end{Bmatrix} + \begin{bmatrix} \mathbf{C}^s_{ii} & \mathbf{C}^s_{ib} \\ \mathbf{C}^s_{bi} & \mathbf{C}^s_{bb} \end{bmatrix} \begin{Bmatrix} \dot{\mathbf{q}}^s_i \\ \dot{\mathbf{q}}^s_b \end{Bmatrix} + \begin{bmatrix} \mathbf{K}^s_{ii} & \mathbf{K}^s_{ib} \\ \mathbf{K}^s_{bi} & \mathbf{K}^s_{bb} \end{bmatrix} \begin{Bmatrix} \mathbf{q}^s_i \\ \mathbf{q}^s_b \end{Bmatrix} = \begin{Bmatrix} \mathbf{f}^s_i \\ \mathbf{f}^s_b \end{Bmatrix} + \begin{Bmatrix} 0 \\ \mathbf{g}^s_b \end{Bmatrix} \tag{2}$$

where subscript i and b denotes the internal and boundary DoFs and superscript s denotes the pertinent substructure s. The schematic diagram detailing the substructure nodes can be found in Figure 1.

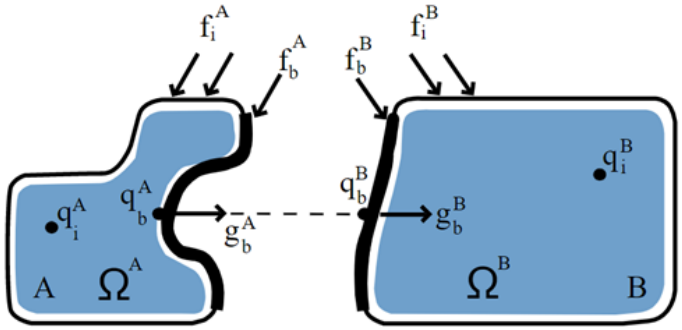

Figure 1: Schematic diagram of substructuring approach with associated DoFs.

The equivalence and continuity between $\mathbf{\Omega}$ and $\mathbf{\Omega}^s$ can be ensured through compatibility and equilibrium conditions. While compatibility ensures that the substructures have identical displacements in the connected DoFs, the force equilibrium condition enforces that the forces at the boundary DoFs of neighbouring substructures balance out each other. From Equation (2), the dynamics for the domain, $\mathbf{\Omega}^{s_i}$, corresponding to the internal DoFs, can further be decoupled from the boundary DoFs as:

$$\mathbf{M}^s_{ii}\ddot{\mathbf{q}}^s_i + \mathbf{C}^s_{ii}\dot{\mathbf{q}}^s_i + \mathbf{K}^s_{ii}\mathbf{q}^s_i = \mathbf{f}^s_i \; - \mathbf{M}^s_{ib}\ddot{\mathbf{q}}^s_b - \mathbf{C}^s_{ib}\dot{\mathbf{q}}^s_b - \mathbf{K}^s_{ib}\mathbf{q}^s_b \tag{3}$$

with the right side of Equation (3) collectively considered as external force acting on Ω^{s_i}. The motion of the internal DoFs, i.e., $\mathbf{q}^s_i(t)$, can further be represented as a summation of a quasi-static ($\mathbf{q}^{s,d}_i$) and a relative ($\mathbf{q}^{s,r}_i$) component [17], wherein the quasi-static component ($\mathbf{q}^{s,d}_i$) provides a rigid body motion to the subdomain Ω^{s_i} and relative component ($\mathbf{q}^{s,r}_i$) enables relative (/flexible) motion. Thereby, the overall response can be defined as:

$$\mathbf{q}^s_i = \mathbf{q}^{s,r}_i + \mathbf{q}^{s,d}_i \tag{4}$$

$\mathbf{q}^{s,d}_i$ can further be obtained by forcing all the force components and time-derivative terms in Equation (3) to zero while assuming the boundary to be free, as

$$\mathbf{q}^{s,d}_i = -\mathbf{K}^{s\,-1}_{ii}\mathbf{K}^s_{ib}\mathbf{q}^s_b = \; \eta^s\mathbf{q}^s_b \tag{5}$$

with η^s acting as a transmissibility term correlating boundary to internal responses. Further, substituting $\mathbf{q}^s_i(t)$ in Equation (3), the following can be obtained,

$$\mathbf{M}_{ii}^{s}(\ddot{\mathbf{q}}_{i}^{s,r}+\ddot{\mathbf{q}}_{i}^{s,d})+\mathbf{C}_{ii}^{s}(\dot{\mathbf{q}}_{i}^{s,r}+\dot{\mathbf{q}}_{i}^{s,d})+\mathbf{K}_{ii}^{s}(\mathbf{q}_{i}^{s,r}+\mathbf{q}_{i}^{s,d})=\mathbf{f}_{i}^{s}\ -\mathbf{M}_{ib}^{s}\ddot{\mathbf{q}}_{b}^{s}-\mathbf{C}_{ib}^{s}\dot{\mathbf{q}}_{b}^{s}-\mathbf{K}_{ib}^{s}\mathbf{q}_{b}^{s} \tag{6}$$

Next, the relative dynamics of the substructure can be isolated from the above equation by considering all terms pertinent to the rigid dynamics of the substructure as an external force and subsequently addressing them jointly with external and resisting forces (right side of Equation (6)).

$$\mathbf{M}_{ii}^{s}\ddot{\mathbf{q}}_{i}^{s,r}+\mathbf{C}_{ii}^{s}\dot{\mathbf{q}}_{i}^{s,r}+\mathbf{K}_{ii}^{s}\mathbf{q}_{i}^{s,r}=\mathbf{f}_{i}^{s}\ -\mathbf{M}_{ib}^{s}\ddot{\mathbf{q}}_{b}^{s}-\mathbf{C}_{ib}^{s}\dot{\mathbf{q}}_{b}^{s}-\mathbf{K}_{ib}^{s}\mathbf{q}_{b}^{s}-\mathbf{M}_{ii}^{s}\ddot{\mathbf{q}}_{i}^{s,d}-\mathbf{C}_{ii}^{s}\dot{\mathbf{q}}_{i}^{s,d}-\mathbf{K}_{ii}^{s}\mathbf{q}_{i}^{s,d} \tag{7}$$

Because of the general nature of a typical linearly damped mechanical system, its system matrices are banded and sparse leading to very feeble interaction between two distant nodes. With internal and boundary nodes segregated, the insignificant off-diagonal terms associated with cross-coupling between these distant node sets, i.e., internal and boundary nodes, therefore, can be ignored without affecting the generality. Moreover, the impact of the ignored part of damping will surely be overshadowed by the noise which is more significant, as verified later on. Thus, the minuscule damping can be ignored in the modeling and can still be accounted for in the model by including it in the modeling error process. Thereby, the insignificant amount of damping force, i.e. $(\mathbf{C}_{ii}^{s}\dot{\mathbf{q}}_{i}^{s,d}+\mathbf{C}_{ib}^{s}\dot{\mathbf{q}}_{b}^{s})$ has been considered under the process uncertainty (discussed later) and removed from the dynamics from now on.

$$\mathbf{M}_{ii}^{s}\ddot{\mathbf{q}}_{i}^{s,r}+\mathbf{C}_{ii}^{s}\dot{\mathbf{q}}_{i}^{s,r}+\mathbf{K}_{ii}^{s}\mathbf{q}_{i}^{s,r}=\mathbf{f}_{i}^{s}\ -\mathbf{M}_{ib}^{s}\ddot{\mathbf{q}}_{b}^{s}-\mathbf{K}_{ib}^{s}\mathbf{q}_{b}^{s}-\mathbf{M}_{ii}^{s}\ddot{\mathbf{q}}_{i}^{s,d}-\mathbf{K}_{ii}^{s}\mathbf{q}_{i}^{s,d} \tag{8}$$

Using Equation (5), $\mathbf{q}_{i}^{s,d}$ can be substituted with $\mathbf{q}_{b}^{s}$ as,

$$\mathbf{M}_{ii}^{s}\ddot{\mathbf{q}}_{i}^{s,r}+\mathbf{C}_{ii}^{s}\dot{\mathbf{q}}_{i}^{s,r}+\mathbf{K}_{ii}^{s}\mathbf{q}_{i}^{s,r}=\mathbf{f}_{i}^{s}\ -\mathbf{M}_{ib}^{s}\ddot{\mathbf{q}}_{b}^{s}-\mathbf{K}_{ib}^{s}\mathbf{q}_{b}^{s}-\mathbf{M}_{ii}^{s}\eta^{s}\ddot{\mathbf{q}}_{b}^{s}+\mathbf{K}_{ii}^{s}{\mathbf{K}_{ii}^{s}}^{-1}\mathbf{K}_{ib}^{s}\mathbf{q}_{b}^{s} \tag{9}$$

and, further can be simplified as,

$$\mathbf{M}_{ii}^{s}\ddot{\mathbf{q}}_{i}^{s,r}+\mathbf{C}_{ii}^{s}\dot{\mathbf{q}}_{i}^{s,r}+\mathbf{K}_{ii}^{s}\mathbf{q}_{i}^{s,r}=\mathbf{f}_{i}^{s}-(\mathbf{M}_{ib}^{s}+\mathbf{M}_{ii}^{s}\eta^{s})\ddot{\mathbf{q}}_{b}^{s} \tag{10}$$

2.2. State-space formulation of substructure

Finally, the system dynamics defined in physical space can be cast in the corresponding state-space as,

$$\dot{\mathbf{x}}^{s}(t)=\mathbf{F}^{s}(t)\,\mathbf{x}^{s}(t)+\mathbf{B}^{s}(t)\,\mathbf{u}^{s}(t)+\ \mathbf{E}^{s}(t)\,\ddot{\mathbf{q}}_{b}^{s}(t)+\mathbf{v}^{s}(t) \tag{11}$$

where, $\mathbf{x}^{s}(t)=\begin{Bmatrix}\mathbf{q}_{i}^{s,r}\\ \dot{\mathbf{q}}_{i}^{s,r}\end{Bmatrix}$, $\mathbf{F}^{s}(t)=\begin{bmatrix}\mathbf{0}_{n_i} & \mathbf{I}_{n_i}\\ -{\mathbf{M}_{ii}^{s}}^{-1}\mathbf{K}_{ii}^{s} & -{\mathbf{M}_{ii}^{s}}^{-1}\mathbf{C}_{ii}^{s}\end{bmatrix}$, $\mathbf{B}^{s}(t)=\begin{bmatrix}\mathbf{0}_{n_i}\\ {\mathbf{M}_{ii}^{s}}^{-1}\end{bmatrix}$, $\mathbf{u}^{s}(t)=\mathbf{f}_{i}^{s}$ and $\mathbf{E}^{s}(t)=\begin{bmatrix}\mathbf{0}_{n_i}\\ -({\mathbf{M}_{ii}^{s}}^{-1}\mathbf{M}_{ib}^{s}+\eta^{s})\end{bmatrix}$.

The additional term $\mathbf{v}^s(t)$ represents process uncertainty (due to modeling inaccuracies, unmodelled input, and damping, etc.), which is modeled as a stationary white Gaussian noise (SWGN) of constant covariance $\mathbf{Q}^v$. The measurable acceleration responses $\ddot{\mathbf{q}}_i^s$ correspond to total acceleration due to pseudo-static ($\ddot{\mathbf{q}}_b^{s,d}$) and relative ($\ddot{\mathbf{q}}_b^{s,r}$) response components combined as $\mathbf{y}^s(t)$.

$$\mathbf{y}^s(t) = S\{\ddot{\mathbf{q}}_i^{s,r}(t) + \eta^s \ddot{\mathbf{q}}_b^s(t)\} = S\{\mathbf{H}^s(t)\mathbf{x}^s(t) + \mathbf{D}^s(t)\mathbf{u}^s(t) + \mathbf{L}^s(t)\ddot{\mathbf{q}}_b^s(t) + \mathbf{w}^s(t)\} \tag{12}$$

where $\mathbf{H}^s(t) = \begin{bmatrix} -\mathbf{M}_{ii}^{s\,-1}\mathbf{K}_{ii}^s & -\mathbf{M}_{ii}^{s\,-1}\mathbf{C}_{ii}^s \end{bmatrix}$, $\mathbf{D}^s(t) = \mathbf{M}_{ii}^{s\,-1}$, and $\mathbf{L}^s(t) = -\mathbf{M}_{ii}^{s\,-1}\mathbf{M}_{ib}^s$ and $\mathbf{w}^s(t)$ denotes measurement uncertainty, described as SWGN of known statistics, $\mathbf{R}$, as $\mathbf{w}^s(t) \sim \mathcal{N}(0, \mathbf{R})$. S represents the Boolean selection matrix defining the measured DoFs. Since in reality, responses are discretely sampled, Equations (11) and (12) is presented in discrete time with continuous variables reproduced with their corresponding discrete-time entities.

$$\begin{aligned} &\text{Process model} \quad : \quad \mathbf{x}_k^s = \mathbf{F}_k^s\mathbf{x}_{k-1}^s + \mathbf{B}_k^s\mathbf{u}_k^s + \mathbf{E}_k^s\ddot{\mathbf{q}}_{b,k}^s + \mathbf{v}_k^s \\ &\text{Measurement model} \quad : \quad \mathbf{y}_k^s = \mathbf{H}_k^s\mathbf{x}_k^s + \mathbf{D}_k^s\mathbf{u}_k^s + \mathbf{L}_k^s\ddot{\mathbf{q}}_{b,k}^s + \mathbf{w}_k^s \end{aligned} \tag{13}$$

Selection matrix S has been dropped from the formulation assuming its impact has been adopted in the discrete-time matrices.

2.3. Interface robustness

With the aforementioned substructure system definition, the approach toward achieving interface robustness is discussed next. Developed with an intent to reject the impact of noise of unknown statistics from the state evolution, the output injection technique [39] has been exploited for eliminating the requirement of the interface measurements in this approach. By suitably injecting a part of the measured output ($\mathbf{y}_k^s$) into the state transition model, the imperative requirement of interface measurement can be alleviated. Owing to the measurement equation (cf. Equation (13)), the following holds true for an arbitrary bounded matrix $\mathbf{G}_k^s \in \mathbb{R}$.

$$\mathbf{0} = \mathbf{G}_k^s\left(\mathbf{y}_k^s - \mathbf{H}_k^s\mathbf{x}_k^s - \mathbf{D}_k^s\mathbf{u}_k^s - \mathbf{L}_k^s\ddot{\mathbf{q}}_{b,k}^s - \mathbf{w}_k^s\right) \tag{14}$$

Adding Equation (14) to Equation (13) and further setting $\mathcal{L}_k^s = \mathbf{I} - \mathbf{G}_k^s\mathbf{H}_k^s$, process model equation (cf. Equation (13)) can be modified as,

$$\begin{aligned} \mathbf{x}_k^s =& \mathbf{F}_k^s\mathbf{x}_{k-1}^s + \mathbf{B}_k^s\mathbf{u}_k^s + \mathbf{E}_k^s\ddot{\mathbf{q}}_{b,k}^s + \mathbf{v}_k^s + \mathbf{G}_k^s\left(\mathbf{y}_k^s - \mathbf{H}_k^s\mathbf{x}_k^s - \mathbf{D}_k^s\mathbf{u}_k^s - \mathbf{L}_k^s\ddot{\mathbf{q}}_{b,k}^s - \mathbf{w}_k^s\right) \\ =& \widetilde{F}_k^s\mathbf{x}_{k-1}^s + \widetilde{B}_k^s\mathbf{u}_k^s + \widetilde{E}_k^s\ddot{\mathbf{q}}_{b,k}^s + \mathbf{G}_k^s\mathbf{y}_k^s + \widetilde{\mathbf{v}}_k^s \end{aligned} \tag{15}$$

with $\widetilde{F}_k^s = \mathcal{L}_k^s\mathbf{F}_k^s, \widetilde{B}_k^s = \mathcal{L}_k^s\mathbf{B}_k^s - \mathbf{G}_k^s\mathbf{D}_k^s, \widetilde{E}_k^s = \mathcal{L}_k^s\mathbf{E}_k^s - \mathbf{G}_k^s\mathbf{L}_k^s$, and $\widetilde{\mathbf{v}}_k^s = \mathcal{L}_k^s\mathbf{v}_k^s - \mathbf{G}_k^s\mathbf{w}_k^s$. If $\mathbf{G}_k^s$ is chosen such that $\mathbf{G}_k^s = \mathbf{E}_k^s(\mathbf{H}_k^s\mathbf{E}_k^s + \mathbf{L}_k^s)^\dagger$ with $\dagger$ denoting Moore-Penrose Pseudo-inverse operation, $\widetilde{E}_k^s$ renders to

a null matrix. Equation (15) is then transformed to Equation (16), with no dependency on the boundary measurements, $\ddot{\mathbf{q}}^s_{b,k}$, as,

$$\mathbf{x}^s_k = \widetilde{F}^s_k \mathbf{x}^s_{k-1} + \widetilde{B}^s_k \mathbf{u}^s_k + \mathbf{G}^s_k \mathbf{y}^s_k + \widetilde{\mathbf{v}}^s_k \tag{16}$$

with, Equation (16) showing the dependence of $\mathbf{x}^s_k$ on known states ($\mathbf{x}^s_{k-1}$), and internal DoF measured response, $\mathbf{y}^s_k$, only. Thus, with the proposed approach, states of substructure s can be estimated without measuring the interface response.

However, the measurement equation, as in Equation (13), is dependent on the unknown interface response. To alleviate this, the measurement equation has been transformed through pre-multiplying with a suitably chosen matrix $\mathbf{T}^s_k$ such that $\mathbf{T}^s_k \mathbf{L}^s_k = 0$. This leads to the following transformed measurement equation,

$$\mathbf{z}^s_k = \widetilde{H}^s_k \mathbf{x}^s_k + \widetilde{D}^s_k \mathbf{u}^s_k + \widetilde{w}^s_k \tag{17}$$

wherein, $\mathbf{z}^s_k = \mathbf{T}^s_k \mathbf{y}^s_k$, $\widetilde{H}_k = \mathbf{T}^s_k \mathbf{H}^s_k$, $\widetilde{D}_k = \mathbf{T}^s_k \mathbf{D}^s_k$ and $\widetilde{w}^s_k = \mathbf{T}^s_k \mathbf{R}$. Eventually, this needs the estimate for the transformation matrix $\mathbf{T}^s_k$ which is the left null space of $\mathbf{L}^s_k$. Taking into account an unknown and unmeasured perturbation in the measurement equation is a novelty compared to past output injection approaches.

3. State and parameter estimation with interacting particle ensemble Kalman filter

The proposed state-space formulation for substructure systems has been described in Section 2. Further, the states and parameters are estimated from the formulated equations with the help of an interacting filtering technique (IPEnKF) [1, 24]. The health of the structure is parameterized with p_s number of location-based health indices (**HI**s), which are estimated using a set of particles ($\boldsymbol{\xi}$) with PF. **HI** is defined as the reduction in the flexural rigidity of the element, $(EI)^d_k = \xi.(EI)^0_k$, from its initial health state, $(EI)^0_k$. This allows monitoring health corresponding p_s locations of the structure rendering the monitoring resolution depending on p_s. The state ($\mathbf{x}^s_k$) estimation is further approached through EnKF which is nestled within the PF. The current health estimates are employed to define the current state/system or measurement/output matrices, and thereby both filters interact with each other leading to state estimates conditional to the health estimates.

PF employs a crude sample-based uncertainty propagation approach wherein the prior estimates are propagated through the state evolution equation using N_p independent particles ($\boldsymbol{\xi}_{p_s \times 1}$), each of which can be considered as a realization of the multivariate random variable **HI**. Accordingly, at k^{th} time step, the prior parameter estimates (and associated uncertainties) are propagated through a state evolution equation with PF using a set of parameter particles $\boldsymbol{\xi} = [\xi^1_{k-1}, \xi^2_{k-1}, \cdots, \xi^{N_p}_{k-1}]_{p_s \times N_p}$. During time evolution, each

of the particles (ξ_{k-1}^j) evolve through random perturbations around their current position. A Gaussian blurring is performed on ξ_{k-1}^j with a shift $\delta\xi_k = (1-\alpha)\bar{\xi}_{k-1}$ and a spread of σ_k^{ξ} [1]. The turbulence in the particle estimation is controlled with the help of α by re-centering the particles towards their mean ($\bar{\xi}_{k-1}$), given by the following,

$$\xi_k^j = \alpha\xi_{k-1}^j + \mathcal{N}(\delta\xi_k, \sigma_k^{\xi}) \tag{18}$$

Eventually, the particles are evolved based on their likelihood against the current time-step measurement. Thus, the particle evolution becomes independent of the initial distribution assumed for $\boldsymbol{\xi}$. Embedded EnKF for state estimation is then applied to the propagated particles in order to estimate the likelihood.

For each j^{th} particle, EnKF propagates N_e state ensembles through the system model (cf. Equation (16)) conditioned on the current parameter estimate (ξ_k^j from Equation (18)). The predicted value of the states ($\mathbf{x}_{k|k-1}^{i,j}$) and transformed measurement ($\mathbf{z}_{k|k-1}^{i,j}$) corresponding to j^{th} particle and i^{th} ensemble is given by,

$$\begin{aligned}
\mathbf{x}_{k|k-1}^{i,j} &= \widetilde{F}_k^{i,j}\mathbf{x}_{k-1|k-1}^{i,j} + \widetilde{B}_k^{i,j}\mathbf{u}_k^{i,j} + \mathbf{G}_k^{i,j}\mathbf{y}_k + \widetilde{\mathbf{v}}_k^{i,j} \\
\mathbf{z}_{k|k-1}^{i,j} &= \widetilde{H}_k^{i,j}\mathbf{x}_{k|k-1}^{i,j} + \widetilde{D}_k^{i,j}\mathbf{u}_k^{i,j} + \widetilde{w}_k^{i,j}
\end{aligned} \tag{19}$$

It should be noted that, from here on, superscript s is dropped for better readability. Further, innovation for i^{th} ensemble is calculated as the departure of predicted transformed measurement from the output transformed measurement sensor data $\varepsilon_k^{i,j} = \mathbf{z}_k - \mathbf{z}_{k|k-1}^{i,j}$. The overall innovation is computed as $\varepsilon_k^j = \frac{1}{N_e}\sum_{i=1}^{N_e}\varepsilon_k^{i,j}$. The predicted state and transformed measurement error covariance, $C_k^{j,xz}$, and the transformed measurement error covariance ($\mathbf{S}_k^j$) is given by,

$$\begin{aligned}
C_k^{j,xz} &= \frac{1}{N_e-1}\sum_{i=1}^{N_e}\left(\mathbf{x}_{k|k-1}^{j} - \mathbf{x}_{k|k-1}^{i,j}\right)\left(\mathbf{z}_{k|k-1}^{j} - \mathbf{z}_{k|k-1}^{i,j}\right)^T \\
\mathbf{S}_k^j &= \frac{1}{N_e-1}\sum_{i=1}^{N_e}\left(\mathbf{z}_{k|k-1}^{j} - \mathbf{z}_{k|k-1}^{i,j}\right)\left(\mathbf{z}_{k|k-1}^{j} - \mathbf{z}_{k|k-1}^{i,j}\right)^T + \mathbf{T}_k\mathbf{R}{\mathbf{T}_k}^T
\end{aligned} \tag{20}$$

where, $\mathbf{x}_{k|k-1}^j$ and $\mathbf{z}_{k|k-1}^j$ are the respective ensemble mean of the predicted states and transformed measurement, respectively. From the covariances obtained from Equation (20), EnKF gain is obtained as, $\mathbb{G}_k^j = C_k^{j,xz}(\mathbf{S}_k^j)^{-1}$. Based on the innovation mean, $\varepsilon_k^{i,j}$, and the EnKF gain, $\mathbb{G}_k^j$, the state ensembles are updated as follows,

$$\mathbf{x}_{k|k}^{i,j} = \mathbf{x}_{k|k-1}^{i,j} + \mathbb{G}_k^j\varepsilon_k^{i,j} \tag{21}$$

[1] $A + B\mathbb{N}(\mu,\sigma)$ means $A + Bz$ where z follows $\mathbb{N}(\mu,\sigma)$

Further the likelihood, $\mathcal{L}(\xi_k^j)$, of each particle is also calculated, as $\mathcal{L}(\xi_k^j) = \frac{1}{(2\pi)^n\sqrt{|\mathbf{S}_k^j|}} e^{-0.5{\varepsilon_k^j}^T {\mathbf{S}_k^j}^{-1}\varepsilon_k^j}$. For each j^{th} particle, the normalized weight is computed as follows,

$$w(\xi_k^j) = \frac{w(\xi_{k-1}^j)\mathcal{L}(\xi_k^j)}{\sum_{j=1}^{N_p} w(\xi_{k-1}^j)\mathcal{L}(\xi_k^j)} \tag{22}$$

Finally, particle approximations for states and parameters are estimated as follows,

$$\mathbf{x}_{k|k} = \sum_{j=1}^{N_p} w(\xi_k^j)\mathbf{x}_{k|k}^j \quad \text{and} \quad \boldsymbol{\xi}_{k|k} = \sum_{j=1}^{N_p} w(\xi_k^j)\xi_k^j \tag{23}$$

The proposed approach has been provided as a pseudo-code (cf. Algorithm 1) for the SHM of substructure systems.

Algorithm 1 Proposed SHM algorithm for substructures

procedure IPEnKF($\mathbf{y}_k, \mathbf{Q}, \mathbf{R}$)
  Initialize particles $\{\xi_0^j\}$, and state estimates $\{\mathbf{x}_{0|0}^{i,j}\}$
  for <each k^{th} measurement $\mathbf{y}_k$> **do**
    procedure IP-EnKF($\{\xi_{k-1}^j\}, \{\mathbf{x}_{k-1|k-1}^{i,j}\}$)
      for <each particle ξ_k^j> **do**
        Evolve $\{\xi_{k-1}^j\} \rightarrow \{\xi_k^j\}$ ▷ as per Equation (18)
        procedure EnKF($\xi_k^j, \{\mathbf{x}_{k-1|k-1}^{i,j}\}, \mathbf{y}_k$) ▷ For each j^{th} particle
          for <each ensemble $\mathbf{x}_{k-1|k-1}^{i,j}$> **do**
            Prediction: Propagate state to $\mathbf{x}_{k|k-1}^{i,j}$ ▷ Equation (19)
            Estimate transformed measurement, $\mathbf{z}_{k|k-1}^{i,j}$ ▷ Equation (19)
          end for
          Calculate ensemble mean of $(\mathbf{x}_{k|k-1}^j)$ and $(\mathbf{z}_{k|k-1}^j)$ ▷ as per Section 3
          Evaluate overall innovation (ε_k^j) ▷ as per Section 3
          Compute covariances ($C_k^{j,xz}$ and $\mathbf{S}_k^j$) and EnKF gain ($\mathbb{G}_k^j$) ▷ as per Section 3
          Correction: Correct predicted state estimate ▷ Equation (21)
        end procedure
        Calculate ensemble mean of the corrected state, i.e., $\mathbf{x}_{k|k}^j$
      end for
    end procedure
    procedure Particle re-sampling($\{\xi_k^j\}$)
      For each ξ_k^j, calculate $w(\xi_k^j)$ ▷ Equation (22)
      Update: Update state, $\mathbf{x}_{k|k}$, and parameter estimates, $\boldsymbol{\xi}_{k|k}$, as their weighted mean ▷ Equation (23)
    end procedure
  end for
end procedure

4. Numerical Experiment

The proposed approach has been validated with numerical experiments to establish its efficacy. In this study, the numerical experiment is carried out using a finite element model of a prismatic simply supported beam with geometric properties: span = 3 m, area = 0.013×0.013 m^2, and material properties: mass density (ρ) = 7850 kg/m^3 and elastic modulus (E) = 200 GPa. The numerical model of the beam is divided

into 10 equal parts as elements, with each element being modeled as a two-noded Euler-Bernoulli beam with two DoFs at each node (vertical and rotational). In the following, the usual simulation strategy adopted in this study has been detailed.

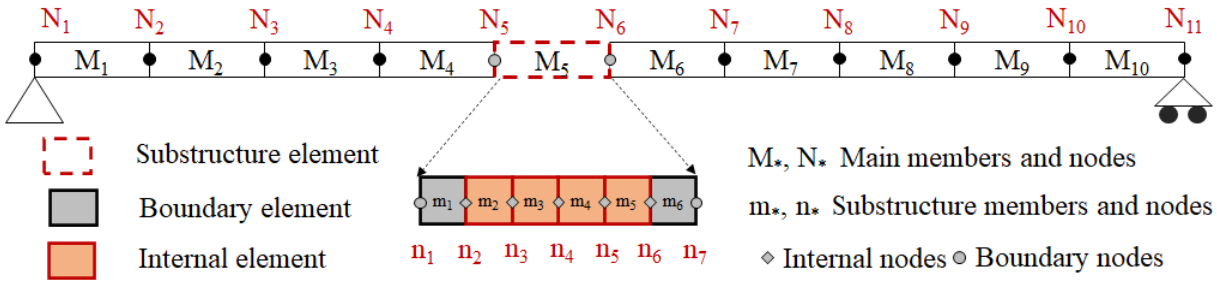

Figure 2: Schematic diagram of a simply supported beam model with its substructure.

The model is simulated under an SWGN forcing ($\mathcal{N}(0, 1e^{-3}N)$) exerted on each DoF (both vertical and rotational) of the structure for a time window of 60 s. Assuming the numerical beam is instrumented at its fifth element/substructure, i.e., M_5, the element is further discretized into six more elements. This leads to the introduction of five internal nodes within element M_5. The simulation recorded the responses at these internal nodes (cf. Figure 2) at a sampling frequency of 50 Hz (i.e. $dt = 0.02\ s$). To mimic real-life scenarios, recorded response measurements are further contaminated with SWGN of signal-to-noise ratio (SNR) of 1%.

For simulating damage scenarios, damage in the beam is introduced by reducing the bending stiffness (EI) of the constituent element/s. The numerical validation has been performed under several operational conditions: reduced instrumentation, plausible damage, noise severities, estimation for a longer time, etc. For each of the cases, the reduction of EI, noise SNR levels, damage location and severity, sensor number, and simulation time have been altered accordingly, while keeping the sampling frequency fixed at 50 Hz.

The proposed approach has ignored the terms in the damping matrix corresponding to cross-coupling between the internal and boundary DoFs assuming them to be insignificant to cause any impact on the estimation. In this study, a comparison is therefore drawn between two scenarios: one with and the other without considering those damping terms. The comparison is presented in Figure 3 wherein it can be verified that the neglected damping terms are in fact very small and therefore should not affect the estimation if neglected. Figure 3b presents the relative error between the presence and absence of damping which corresponds to an SNR ratio of 0.006%, much smaller compared to the minimum level of sensor noise assumed, i.e. 1%.

Initially, the value of the parameters (health indices) is assumed to be unknown for both the undamaged and damaged cases. For system estimation purposes, the parameter's initial distribution is assumed to have a mean of 1 (corresponding to a 100% healthy state) with a 2% variance, i.e., $\mathcal{N}(1, 0.02)$. Meanwhile, the tuning parameter, α is set to 0.99 (cf. Equation (18)) based on previous experience with IPEnKF [24].

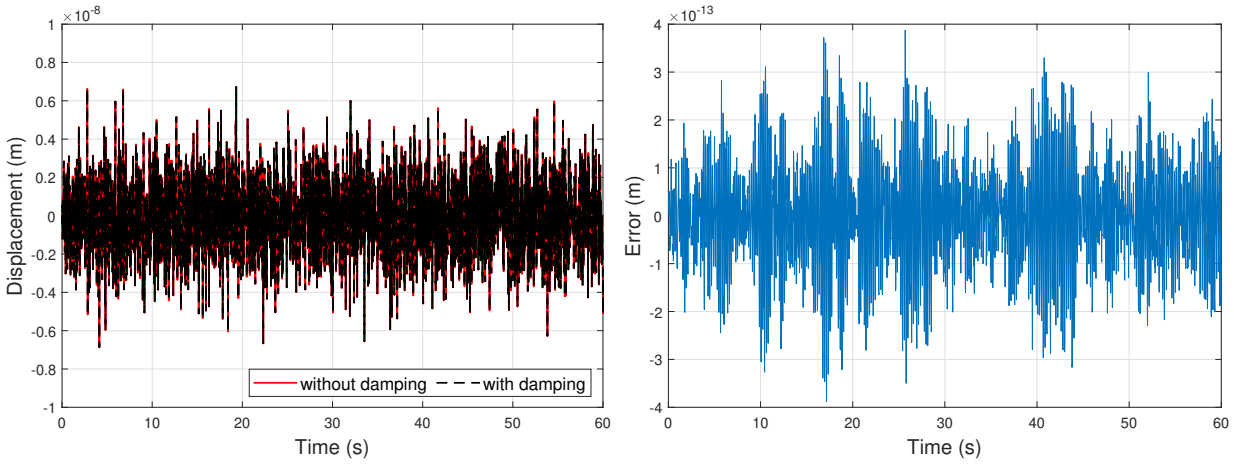

(a) Comparison of displacement

(b) Error between estimated and measured states

Figure 3: Comparison of states corresponding to the presence and absence of damping.

The response recorded from the substructure under consideration (in this case M_5) is used along with the substructured predictor model. For the PF simulation, 2000 particles are used while the EnKF is simulated with 100 ensembles.

4.1. Justification of the proposed algorithm

Prior to the validation of the proposed algorithm, the need for this approach has to be established. For this, the same system response has been processed with four different estimation approaches: 1. The substructured (M_5) model is assumed with fixed end nodes (boundaries), 2. M_5 is assumed with SWGN boundary forces, 3. M_5 is estimated by supplying the actual boundary forces as if they have been measured and finally, 4. M_5 is estimated with the proposed algorithm. For all the cases the simulated measurement response is run through the same IPEnKF strategy, but the substructure support FEM model is different according to the mentioned cases. The comparative study is presented in Figure 4, wherein it can be verified that while with the first two assumptions (cf. Figures 4a and 4b), the estimation of the health indices is not possible, the third assumption yielded prompt and smooth estimation (cf. Figure 4c). However, for the fourth experiment which avoids the boundary estimation (cf. Figure 4d), the results are found to be similar to the case when the actual boundary measurements are supplied (case 3). This illustrates that the proposed method has successfully alleviated the requirement of boundary response measurement without sacrificing the estimation accuracy.

The predicted measurements obtained from the estimated states with the proposed approach are further compared with their actual values obtained during simulation. Figure 5a presents the comparison between the true states and their estimation with the proposed approach. Figure 5b depicts the relative difference between the measured and estimated acceleration which corresponds to an SNR of 0.9%. Considering that uncorrelated uncertainties originating from multiple sources are additive, a significant modelling error would

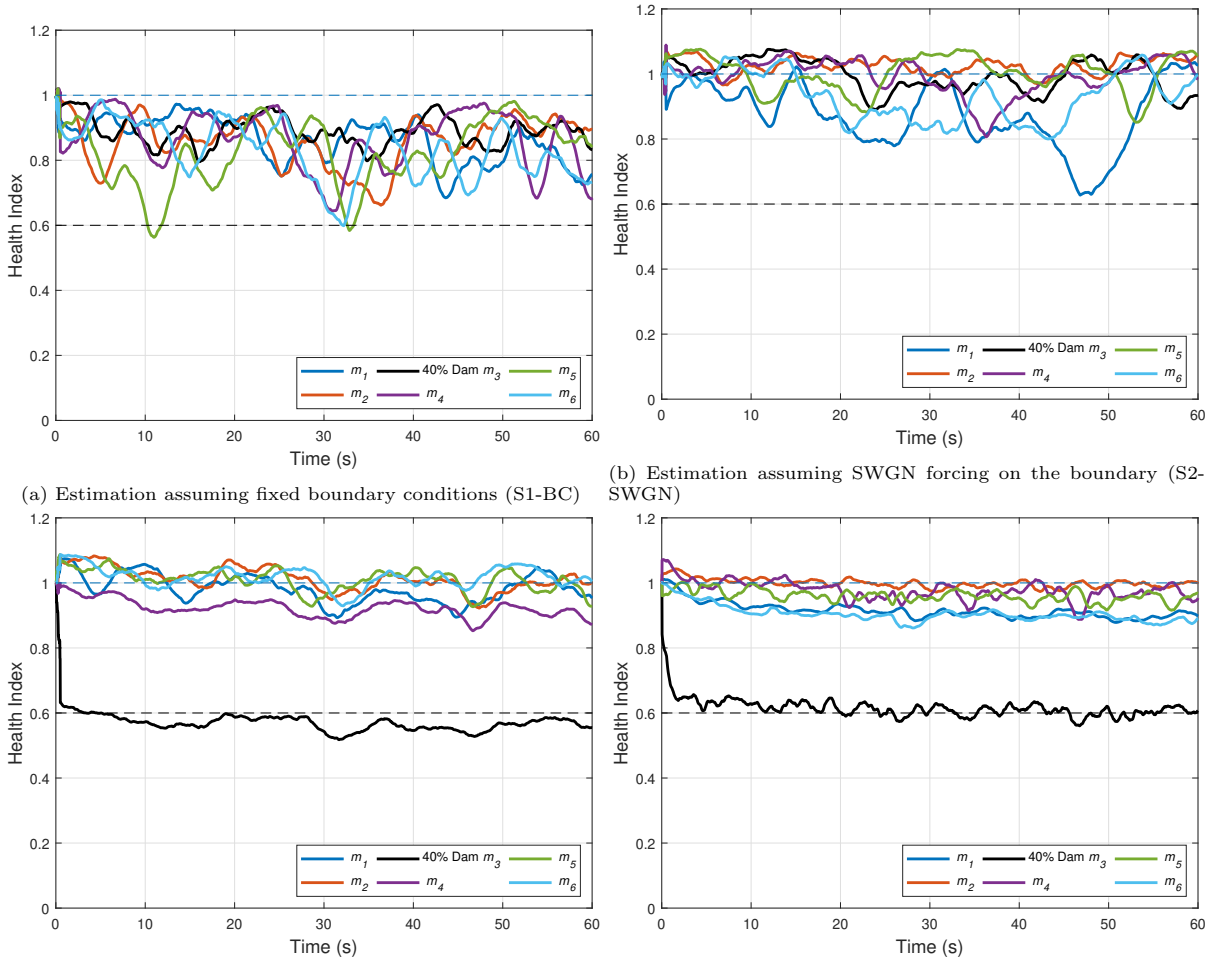

(a) Estimation assuming fixed boundary conditions (S1-BC)

(b) Estimation assuming SWGN forcing on the boundary (S2-SWGN)

(c) Estimation with boundary forces as known (S3-BM)

(d) Estimation with the proposed method (S4-ROBUST)

Figure 4: Estimation of health indices under different conditions (*dashed lines represent respective actual values*).

result in an increase of the observed uncertainty above the expected level, i.e. the 1% noise level. Since the estimated SNR is at 0.9% , similar to the noise level, it is deduced that the modelling error can be considered negligible since it does not impact significantly the response estimation and the proposed approach.

4.2. Sensitivity to damage severity

Further, the sensitivity of the proposed algorithm for different levels of damage severity is investigated. For this, four different damage levels are experimented with, i.e. 20%, 40%, 60%, and 80% along with the undamaged condition. Accordingly, the element elasticity of one element of the numerical beam is reduced by the corresponding percentage to simulate damage. It has been perceived that the proposed approach is equally efficient for all the mentioned damage levels while the estimation has been observed to be smoother (less fluctuating) for higher damage levels, cf. Figure 6. Alongside, the undamaged condition has also been detected precisely with no instances of false alarm.

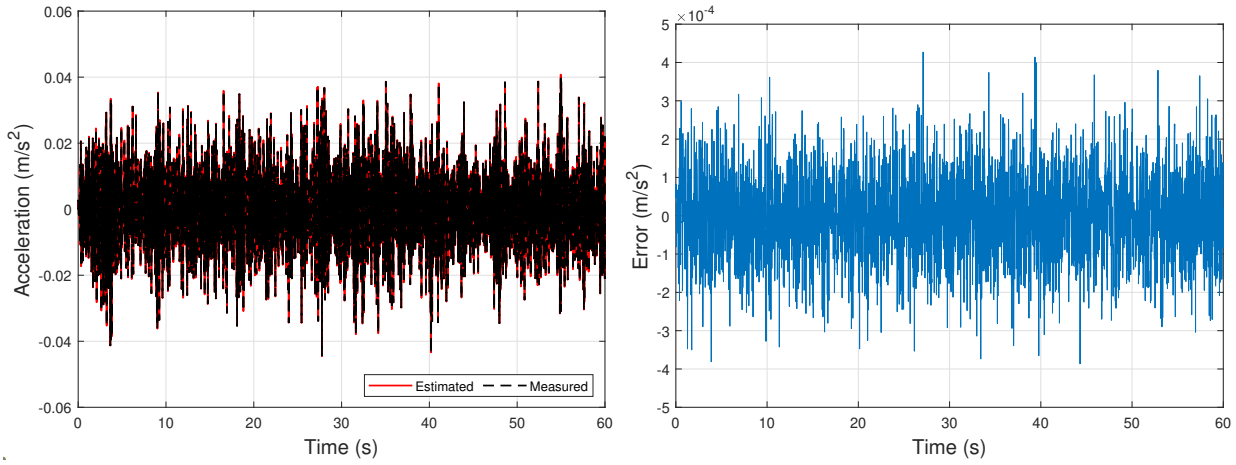

(a) Comparison of acceleration

(b) Error between estimated and measured response

Figure 5: Comparison of reconstructed internal response to the actual measurement response.

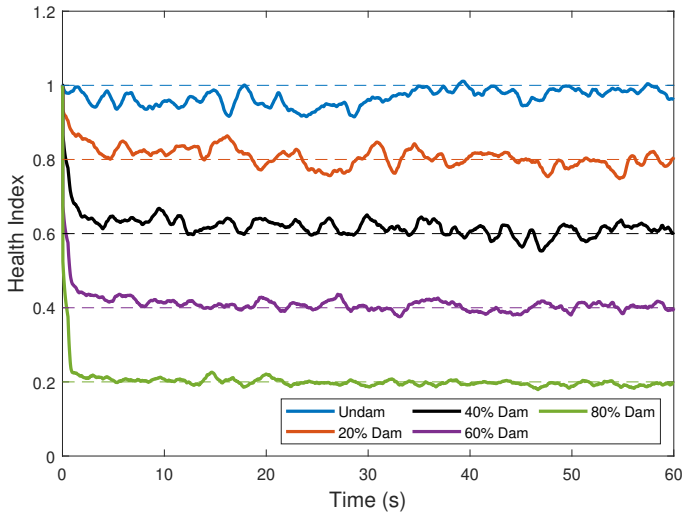

Figure 6: Detection of various damage levels (S5-DQ) in the element m_3 with the proposed approach (*dashed lines represent respective actual values*).

4.3. False alarm sensitivity

Next, the false alarm sensitivity of the algorithm is investigated. In this attempt, two aspects have been emphasized: 1. health deterioration owing to incurred damage/s in the substructure should be detected with precision (this also refers to identifying healthy states causing no false positive alarm and multi-damage scenario causing no false negative alarm) and 2. damage in other parts of the structure should not get confused with damage in the monitored substructure and consequent raising of any false positive alarm. Moreover, the required sensor density to ensure such robustness against false alarms is required to be investigated.

Accordingly, two experiments are firstly performed in which adjacent and distant elements of the mon-

itored substructure are damaged while keeping the domain of concern undamaged. The first experiment assumes damage in the vicinity of the monitored substructure (M_5), i.e., M_4 and M_6 while the second experiment assumes damage in locations (M_2 and M_9) away from the concerned substructure M_5. The results are presented in Figure 7. It can be verified that for both cases, the proposed approach identified the health indices of the monitored substructure M_5 and was not confused by the presence of damage elsewhere in the structure. A separate case study (cf. Table 1) is also undertaken wherein two adjacent elements are damaged: one within the monitored substructure (m_5) while the other outside (M_6) the monitored domain. The proposed approach is observed to detect damage in the monitored element without being deterred by the damage in the adjacent element.

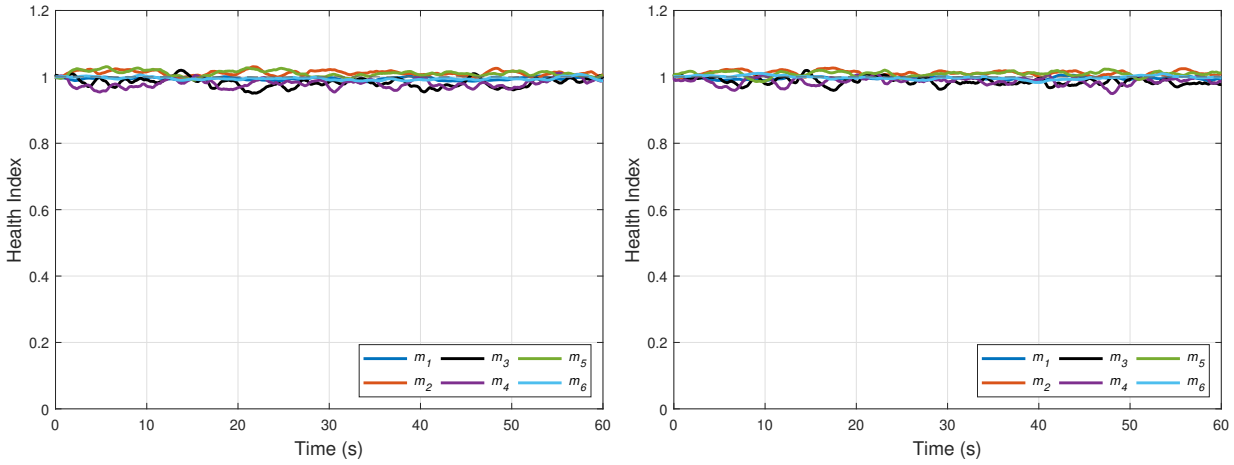

(a) With 40% damage in M_4 and M_6

(b) With 40% damage in M_2 and M_9

Figure 7: False alarm sensitivity (S6-DL) with near and far damage locations (*dashed lines represent respective actual values*).

The capability of the proposed algorithm to assess health under multiple damages within the substructure has also been envisaged in order to establish that the proposed method can identify the location and severity of damage distinctly without suppression or false detection of damage elsewhere within the monitored substructure. The estimation results are presented in Figure 8a which establishes that the proposed approach performs efficiently even with multiple damage scenarios without failure.

Moreover, a separate experiment is also performed under different instrumentation densities: a number of 6, 8, and 10 of measurement channels are therefore employed for the estimation (cf. Figure 8b). It should be noted that since a total of four channels of boundary measurements are being rejected in this numerical experimentation, the employment of a minimum of five channels of measurement becomes imperative. Accordingly, the minimum number of channels for the experiment is selected to be 6. However, it has been observed that mere 6 channels render the problem to be very ill-posed leading to missed detection while 8 and 10 channels have successfully estimated the location and severity of stiffness deterioration.

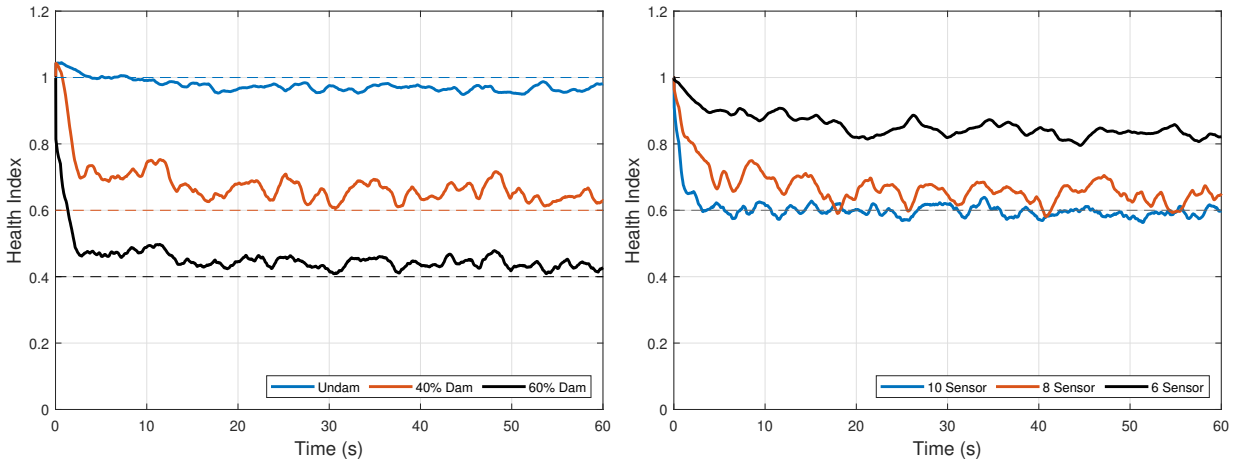

(a) Health assessment under multiple damage scenario (S7-DD)

(b) Sensitivity to instrumentation density (S8-NIS)

Figure 8: Performance of the proposed algorithm under different operating scenarios (*dashed lines represent respective actual values*).

4.4. Noise severity

The noise severity has been investigated under four different noise levels, i.e., 1%, 2%, 5%, and 10% SNR. As expected, it has been observed (cf. Figure 9a) that while the proposed algorithm has been successful in identifying deteriorating health under the mentioned noise severity levels, higher noises are perceived to cause more fluctuations in the estimation. Further, the stability of the algorithm has been tested by subjecting it to longer time series data and the pertinent results are presented in Figure 9b. The health estimation has been observed to be non-divergent and smooth even for prolonged usage, with no evidence of error accumulation or instability. The temporal variation of particles (health indices) corresponding to both damaged and undamaged elements has been plotted with a 95% confidence interval for a better understanding of the Bayesian filtering-based approach.

The performance of the proposed approach in terms of estimated **HI** and corresponding error has been summarized in Table 1 for the case studies undertaken. The estimation means over the last 100 iterations for **HI**s along with their respective root mean square error (RMSE) are presented in Table 1.

5. Experimental validation - fixed beam

A laboratory experiment has been conducted on a fixed-fixed steel beam of a rectangular cross-section to evaluate the performance of the proposed algorithm on real-life structures. The relevant geometric properties as adopted are: span = 1.5 m, area = 261.45 mm^2, with depth 8.3 mm and a very rough estimate of the initial material properties: mass density (ρ) = 7850 kg/m^3 and elastic modulus (E) = 190 GPa. The beam is held in place by clamping both ends, which is then numerically replicated by assuming fixed-fixed boundary conditions. The proposed model-based health assessment approach replicates the real beam numerically

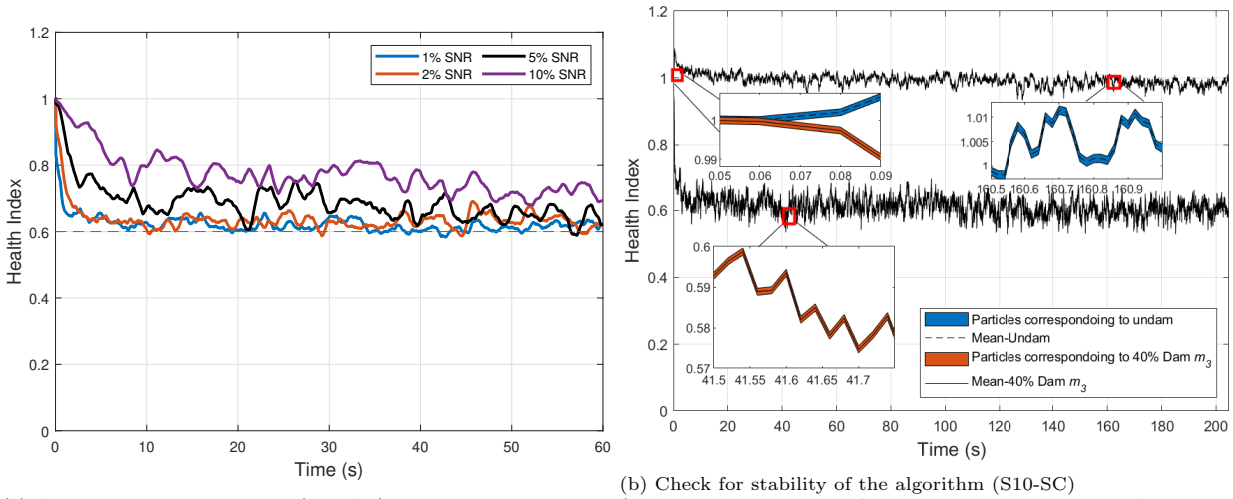

(a) Sensitivity to noise severity (S9-NST)
(*The dashed line represents the actual* ***HI***)

(b) Check for stability of the algorithm (S10-SC)
(*The insets in the right figure present the evolution of HIs corresponding to one damaged and one undamaged element.*)

Figure 9: Noise sensitivity and stability performance of the proposed algorithm

Table 1: Summarised performance of the proposed method under different scenarios.

Scenario name	N_{s_i}	$\mathbf{HI}_{act}$ (internal)	D_l	SNR (%)	D_a	$\mathbf{HI}_{est}$ (mean) (internal)	Error (RMSE)
S1-BC	10	0.6	m_3	1	×	–	
S2-SWGN	10	0.6	m_3	1	×	–	
S3-BM	10	0.6	m_3	1	✓	0.57	0.06
S4-ROBUST	10	0.6	m_3	1	✓	0.61	0.02
S5-DQ	10	1	m_3	1	✓	0.97	0.04
	10	0.8	m_3	1	✓	0.82	0.03
	10	0.4	m_3	1	✓	0.40	0.02
	10	0.2	m_3	1	✓	0.20	0.01
S6-DL	10	1	M_2 & M_9	1	✓	0.98	0.02
	10	1	M_4 & M_6	1	✓	0.99	0.02
	10	0.2	m_5 & M_6	1	✓	0.29	0.14
S7-DD	10	0.6 in m_3 & 0.4 in m_4		1	✓	0.63 & 0.43	0.04 & 0.03
S8-NIS	8	0.6	m_3	1	✓	0.65	0.05
	6	0.6	m_3	1	✓	0.82	0.22
S9-NST	10	0.6	m_3	2	✓	0.62	0.03
	10	0.6	m_3	5	✓	0.64	0.05
	10	0.6	m_3	10	✓	0.72	0.12
S10-SC	10	0.6	m_3	1	✓	0.61	0.02

Here S1-BC: Substructure boundaries are fixed, S2-SWGN: Substructural boundary measurement as SWGN, S3-BM: Substructure boundary measurement data is known, S4-ROBUST: Proposed substructure with robustness, S5-DQ: Damage quantification, S6-DL: Damage location away from the substructure, S7-DD: Double damage, S8-NIS: Number of interior sensors, S9-NST: Noise sensitivity test, S10-SC: Stability check. N_{s_i} denotes the number of interior sensors, D_l denotes location of damage induced, and D_a denotes the damage assessment.

with a 2D Euler-Bernoulli beam. The experimental beam and its numerical replica (or model) are firstly discretized into three equal parts as component substructures (M_1, M_2, M_3). The second substructure, i.e.,

M_2, is opted for independent health monitoring and is accordingly discretized into five elements. This leads to the introduction of four internal nodes within substructure M_2. The experimental details and schematic for the substructured domain are presented in Figure 10a and Figure 10b.

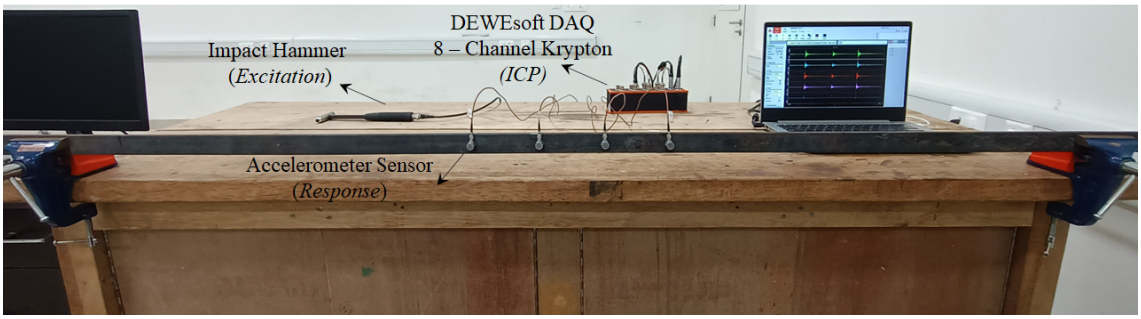

(a) Experimental setup

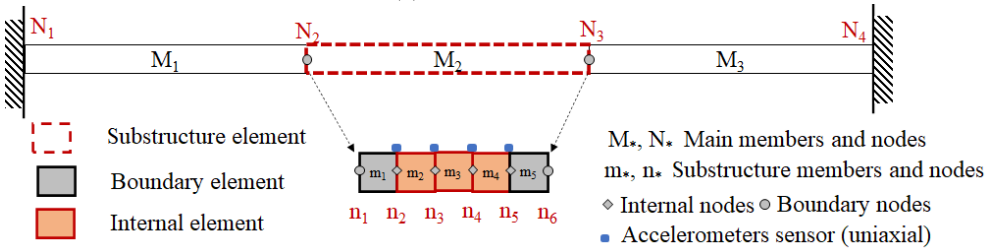

(b) Schematic numerical model of the real beam

Figure 10: Experimental setup - fixed-fixed beam.

5.1. Bench-marking the undamaged beam

It is always advisable to calibrate the basic material properties of the numerical FEM support model with respect to the real structure. Further, it accounts for the non-homogeneous nature of the material property (Elasticity) of the structure. Accordingly, the undamaged beam is excited with an impact load, and the obtained acceleration, sampled at 500 Hz, is used to estimate its frequencies. In this attempt, the material density has been found to be quite consistent with no need for any substantial calibration. However, the estimated frequencies obtained from frequency domain decomposition (FDD) of the recorded response obtained from the beam do not match with the numerically obtained frequencies where the material elasticity is assumed to be uniform throughout the length of the beam. The material elasticity is perturbed to approximately match (within acceptable limits) the numerical frequencies with the ones obtained experimentally (cf. Table 2), and the calibrated uniform elasticity throughout the beam length is estimated as 150 GPa.

The numerical model of the experimental setup is further benchmarked to accommodate the non-homogeneous nature of elasticity in real-life structures. This has been undertaken through the proposed health assessment algorithm. Eventually, this entails the re-calibration of the modulus of elasticity for each of the elements. For this, the substructure M_2 is instrumented with four uni-axial accelerometers placed at

Table 2: Comparison between frequencies obtained experimentally and numerically.

Data		Experimental	Calibrated numerical	Relative error (%)
Frequency (Hz)	ω_1	16.36	16.43	0.43
	ω_2	46.02	45.71	0.67

four equidistant internal nodes fetching structural vibration response only in the vertical DoFs at a sampling frequency of 500 Hz. 100 ensembles and 2000 particles have been selected for IPEnKF with $\alpha = 0.99$ (cf. Equation (18)). Each element elasticity is initiated at 150 GPa which was obtained through the aforementioned calibration approach. The system health is estimated by assuming prior estimates for all the **HI**s as 1 with a standard deviation of 0.02 and subsequently, the algorithm is allowed to update them drawing inference from the time domain response data collected from the known healthy state of the test structure.

This kind of material property calibration can be considered as health indices benchmarking of a structure with an unknown health state. The **HI** estimation results are presented in Figure 11a where it is observed that the **HI**s converged to different values (mostly above 1). The model-predicted measurements are also compared to the actual measurements obtained from the sensors in order to validate the quality of the updated model. Since the experimental beam structure did not have any visible damage, change in the **HI**s has been attributed to an incorrect presumption of the elasticity. Accordingly, the element elasticity of the concerned substructure has been updated (cf. Table 3). This updated model has further been adopted as the undamaged benchmark for the experimental beam.

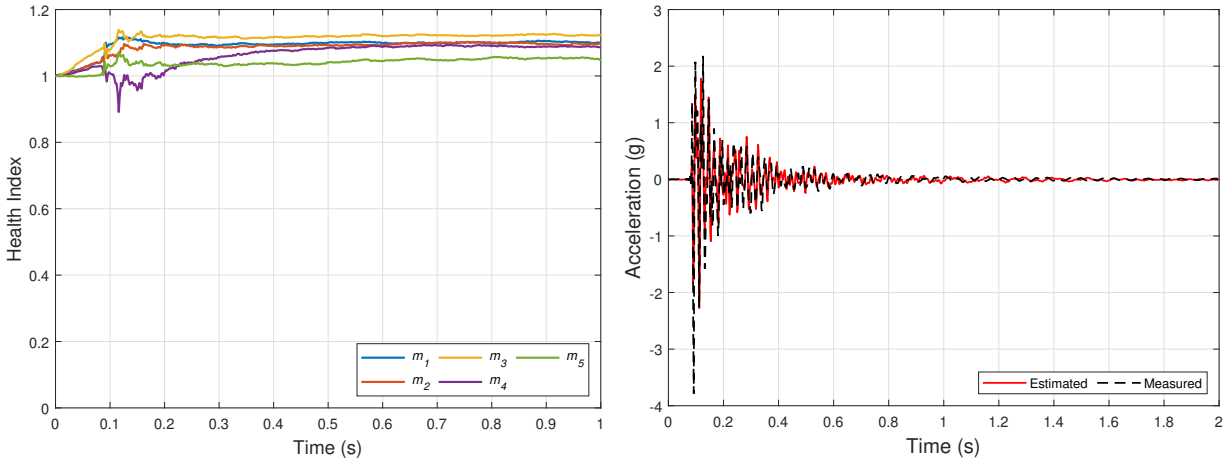

(a) Benchmarking of **HI**s for the undamaged structure

(b) Sensor v/s numerical model predicted measurements

Figure 11: Evaluation of substructure health indices and measurement data comparison for undamaged beam.

5.2. Performance of the proposed algorithm

In the following, the damage has been induced in the third element (m_3) of the second substructure (M_2). The experiment is intended to replicate the local deterioration of the structural material leading to

Table 3: Initial, and benchmarked element elastic moduli.

Elastic modulus (E)	Substructure members				
	m_1	m_2	m_3	m_4	m_5
Initial (GPa)			150.0		
Calibrated (GPa)	165.7	165.4	168.9	164.2	158.3

loss in thickness (e.g. due to spalling and scaling in concrete, corrosion and rusting in steel, etc.). For this, some material from the beam has been scrapped along its depth, reducing the depth of substructure element m_2 down to 7.26 mm (average value over the element length), which can roughly be attributed to 33.08% loss in the element stiffness (**HI** = 0.67). The damage in the m_3 element is shown in Figure 12. The damaged beam has been sampled with four uni-axial accelerometers patched at four internal nodes of the substructure at a constant sampling frequency of 500 Hz for 2 s with the rest of the hyper-parameters (required for the algorithm) being the same as mentioned in Section 5.1.

Figure 12: Experimental setup - damaged structure.

The proposed approach is then employed to estimate the **HI**s corresponding to each of the elements of M_2 substructure without measuring the responses at the substructural boundary nodes (n_1 and n_6, cf. Figure 10b). In accordance with Section 4.1, the assumption of SWGN forcing on the boundaries of substructure, M_2, yields an incorrect estimation of the health indices of the substructural elements, cf. Figure 13a. The health estimation results, presented in Figure 13b, illustrate that the algorithm is capable of estimation and localization of damage without any false alarms. The estimate of the elasticity of substructural element m_3 approximately converges to 0.65 which closely matches its expectation. Further, the **HI** estimation is perceived to be very prompt, with the location of the weakened part getting detected within 0.3 s of its occurrence. The health indicators corresponding to the other non-damaged elements have also been observed to fluctuate below 1 corresponding to non-significant damage (around 10%) which can, however, be ignored from a practical viewpoint and is related to the inherent uncertainty of the statistical algorithm.

5.3. Robustness to boundary conditions

Apart from the application of the proposed algorithm for substructure monitoring, a supplementary contribution of the proposed approach is its capability to alleviate the requirement of exact boundary information. Typically structures are idealized with boundaries like free, fixed, or hinged while reality

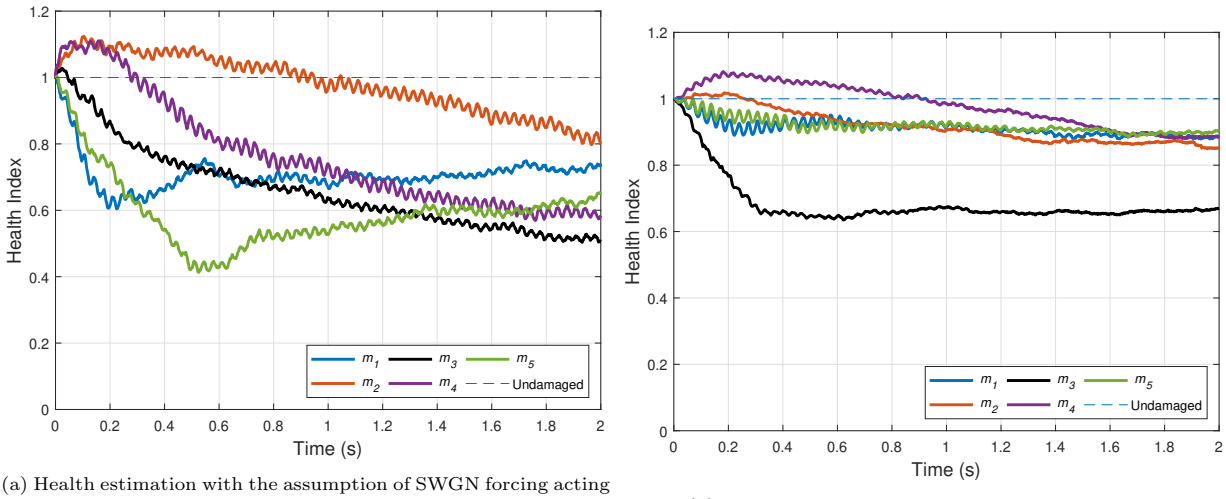

(a) Health estimation with the assumption of SWGN forcing acting on the boundary.

(b) Health estimation with the proposed approach.

Figure 13: Health estimation in the concerned substructure - M_2.

seldom conforms to this idealization. Typically, these boundary fixities have been experienced to behave like a semi-rigid joint wherein the boundary forces or displacements keep on changing during the operation of the structure. Such complex behavior can either be modeled in detail, rendering the predictor model to be complex and computationally inefficient for a recursive estimation platform, or ignored making the algorithm vulnerable to inaccurate and sometimes false estimation (false alarms). However, if the monitoring efficiency can be made independent of such boundary forces, such complications can be averted. With the proposed algorithm, the same can be achieved, detailed next.

To demonstrate this, the experimental focus is shifted from the previously considered substructure to the entire structure. The beam is now simply divided into 5 main elements and 4 uni-axial accelerometers are positioned at the internal nodes as depicted in Figure 14a. The actual clamped fixed boundaries of the beam are considered as the mentioned boundary DoFs in the support FEM model of the proposed approach, cf. Figure 14b with their forces and displacements to be completely unknown to the investigator. Eventually, the model of the test structure considers a free-free beam kept in equilibrium with unknown boundary forces. Keeping all the experimental and algorithm hyper-parameters same as before (cf. Section 5.1), the measurement data is analyzed with the proposed algorithm in order to arrive at the health indices of the discretized elements. Figure 15a shows that the algorithm has promptly detected the instance of health deterioration in the element m_3 as expected, establishing the robustness of the algorithm against the boundary information.

The traditional approach is also applied on the entire structure, which considers the boundary to be fixed, and the results are compared (cf. Figure 15b). It can however be observed that with a presumption of fixity in the boundary, the estimated health is more severe compared to the estimation provided by the proposed approach. Since, through numerical experiments, it has already been established that with the

boundary condition properly known, the proposed approach matches the actual result, it can be concluded that the presumption of the proper fixity was not exactly in the true sense. This obviously signifies the importance of the boundary robustness of the proposed algorithm even for problems wherein the boundary behavior is presumed to be known while the reality does not conform to the presumption. Eventually, with the proposed method, uncertainty caused by boundary conditions is eliminated, making it more accurate than the traditional approach.

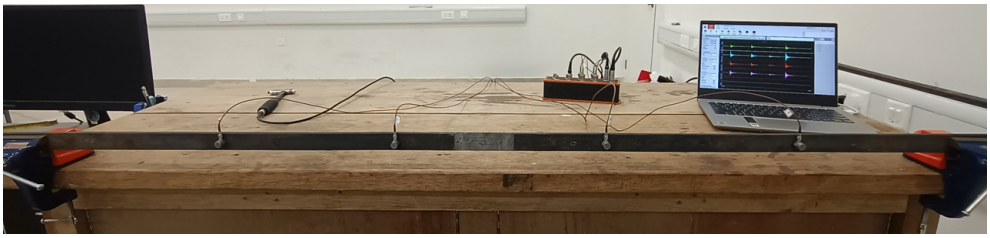

(a) Experimental setup

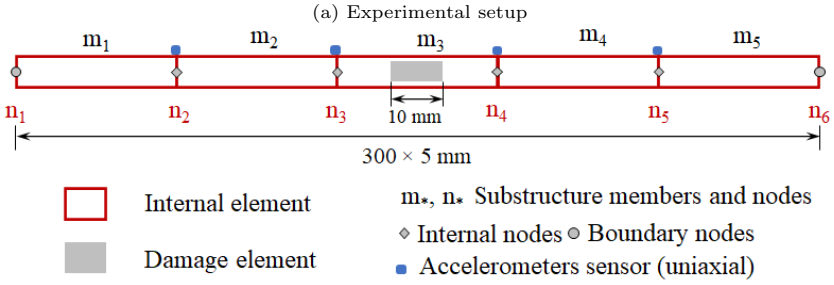

(b) Schematic numerical model of the real beam

Figure 14: Experimental setup - entire structure.

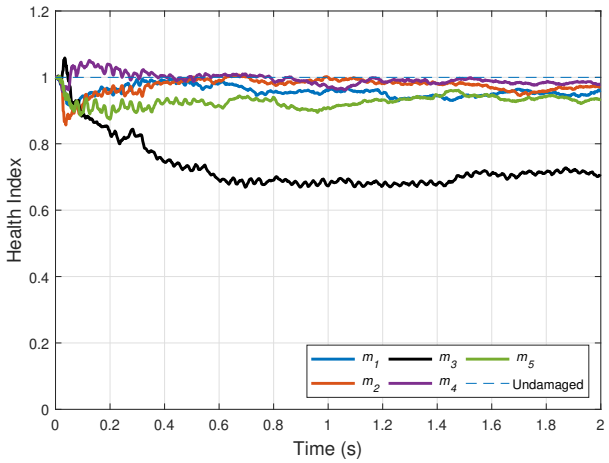

(a) Robustness of the proposed algorithm to boundary conditions

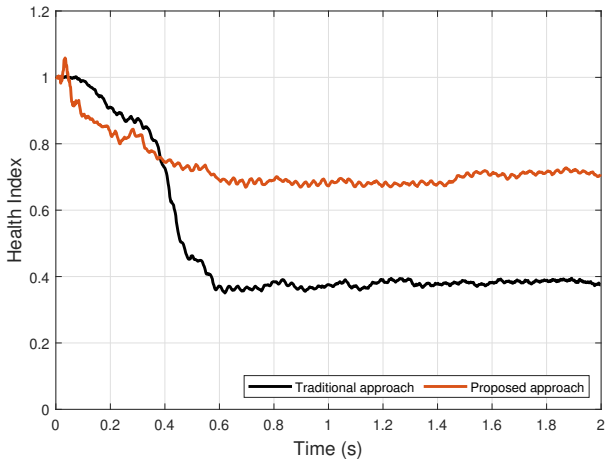

(b) Comparison of traditional and proposed approaches.

Figure 15: Comparison between health estimation of the entire structure using traditional (known boundary conditions) and proposed (unknown boundary conditions) SHM methods.

6. Conclusion

The standard process for estimating the health of a structure and detecting damage employs sensors distributed over the entire structural domain to collect responses. Further model-based approach brings in the additional spatial correlation between the co/non-collocated measurements. However, this traditional approach may be difficult to implement for high-dimensional structures due to the associated computational workload and requirement of dense instrumentation. This article demonstrates a novel Bayesian filter-based approach to alleviate such issues by monitoring only a subdomain of interest in order to achieve computationally cheaper and prompt estimation while instrumenting only a subdomain of interest. The imperative requirement of monitoring the interface boundaries is further avoided through an output injection method, which limits the number of sensors employed for SHM of the substructure to be greater than the rejected interface boundaries. The approach combines two of the most efficient filtering strategies, i.e. PF and EnKF, that allows parallelization of the estimation algorithm. The stand-alone interface independent estimation approach further allows complete parallelization, and consequently, component-wise estimation, which is suitable for distributed health monitoring systems. The proposed approach thereby enables monitoring a large structural domain either by independent estimation of its subdomain in a parallel or sequential approach. Further, the robustness of the proposed algorithm against the unknown boundary condition for full-scale structure is also demonstrated in this attempt. The algorithm has been validated with numerical and real experiments that established the efficacy of the proposed algorithm towards accurate, precise, and prompt detection, localization, and quantification of health deterioration.

Funding: This study was partially funded by Aeronautics Research and Development Board, New Delhi, India, through grant file no. ARDB/01/1052042/M/I.

References

[1] Aswal, N., Sen, S., Mevel, L., 2021. Estimation of local failure in tensegrity using interacting particle-ensemble Kalman filter. Mechanical Systems and Signal Processing 160, 107824.
[2] Chen, Z., et al., 2003. Bayesian filtering: From Kalman filters to particle filters, and beyond. Statistics 182, 1–69.
[3] Ching, J., Beck, J.L., Porter, K.A., 2006. Bayesian state and parameter estimation of uncertain dynamical systems. Probabilistic engineering mechanics 21, 81–96.
[4] Doebling, S.W., Farrar, C.R., Prime, M.B., Shevitz, D.W., 1996. Damage identification and health monitoring of structural and mechanical systems from changes in their vibration characteristics: a literature review .
[5] Fan, W., Qiao, P., 2011. Vibration-based damage identification methods: a review and comparative study. Structural health monitoring 10, 83–111.
[6] Fritzen, C.P., 2005. Vibration-based structural health monitoring–concepts and applications, in: Key Engineering Materials, Trans Tech Publ. pp. 3–20.
[7] Ge, M., Lui, E.M., 2005. Structural damage identification using system dynamic properties. Computers & structures 83, 2185–2196.
[8] Gordon, N.J., Salmond, D.J., Smith, A.F., 1993. Novel approach to nonlinear/non-Gaussian Bayesian state estimation, in: IEE proceedings F (radar and signal processing), IET. pp. 107–113.
[9] Hoshiya, M., Saito, E., 1984. Structural identification by extended Kalman filter. Journal of engineering mechanics 110, 1757–1770.
[10] Hou, J., Jankowski, Ł., Ou, J., 2011. A substructure isolation method for local structural health monitoring. Structural Control and Health Monitoring 18, 601–618.
[11] Hou, J., Jankowski, Ł., Ou, J., 2013. An online substructure identification method for local structural health monitoring. Smart materials and structures 22, 095017.

[12] Huang, M., Cheng, X., Lei, Y., 2021. Structural damage identification based on substructure method and improved whale optimization algorithm. Journal of Civil Structural Health Monitoring 11, 351–380.
[13] Julier, S.J., Uhlmann, J.K., 1997. New extension of the Kalman filter to nonlinear systems, in: Signal processing, sensor fusion, and target recognition VI, International Society for Optics and Photonics. pp. 182–194.
[14] Karlsson, R., Schon, T., Gustafsson, F., 2005. Complexity analysis of the marginalized particle filter. IEEE Transactions on Signal Processing 53, 4408–4411. doi:10.1109/TSP.2005.857061.
[15] Kelly, D.T., Law, K.J., Stuart, A.M., 2014. Well-posedness and accuracy of the ensemble Kalman filter in discrete and continuous time. Nonlinearity 27, 2579.
[16] de Klerk, D., Rixen, D.J., Voormeeren, S., 2008. General framework for dynamic substructuring: history, review and classification of techniques. AIAA journal 46, 1169–1181.
[17] Koh, C., Shankar, K., 2003. Substructural identification method without interface measurement. Journal of engineering mechanics 129, 769–776.
[18] Koh, C.G., See, L.M., Balendra, T., 1991. Estimation of structural parameters in time domain: a substructure approach. Earthquake Engineering & Structural Dynamics 20, 787–801.
[19] Li, Q., Li, R., Ji, K., Dai, W., 2015. Kalman filter and its application, in: 2015 8th International Conference on Intelligent Networks and Intelligent Systems (ICINIS), IEEE. pp. 74–77.
[20] Maes, K., Chatzis, M., Vandebril, R., Lombaert, G., 2021. Observability of modally reduced order models with unknown parameters. Mechanical Systems and Signal Processing 146, 106993.
[21] Mariani, S., Ghisi, A., 2007. Unscented Kalman filtering for nonlinear structural dynamics. Nonlinear Dynamics 49, 131–150.
[22] Mendler, A., Döhler, M., Hille, F., 2022. Detecting changes in boundary conditions based on sensitivity-based statistical tests, in: International Symposium Non-Destructive Testing in Civil Engineering (NDT-CE) in Zurich, Switzerland.
[23] Sabz, A., Reddy, J., Jiao, P., Alavi, A.H., 2019. Structural damage detection using rate of total energy. Measurement 133, 91–98.
[24] Sen, S., Aswal, N., Zhang, Q., Mevel, L., 2021. Structural health monitoring with non-linear sensor measurements robust to unknown non-stationary input forcing. Mechanical Systems and Signal Processing 152, 107472.
[25] Sen, S., Bhattacharya, B., 2016. Progressive damage identification using dual extended Kalman filter. Acta Mechanica 227, 2099–2109.
[26] Sen, S., Bhattacharya, B., 2017. Online structural damage identification technique using constrained dual extended Kalman filter. Structural Control and Health Monitoring 24, e1961.
[27] Sohn, H., Farrar, C.R., Hemez, F.M., Shunk, D.D., Stinemates, D.W., Nadler, B.R., Czarnecki, J.J., 2003. A review of structural health monitoring literature: 1996–2001. Los Alamos National Laboratory, USA 1.
[28] Souid, A., Delaplace, A., Ragueneau, F., Desmorat, R., 2009. Pseudodynamic testing and nonlinear substructuring of damaging structures under earthquake loading. Engineering structures 31, 1102–1110.
[29] Tatsis, K.E., Dertimanis, V.K., Papadimitriou, C., Lourens, E., Chatzi, E.N., 2021. A general substructure-based framework for input-state estimation using limited output measurements. Mechanical Systems and Signal Processing 150, 107223.
[30] Tee, K.F., Koh, C.G., Quek, S.T., 2003. System identification and damage estimation via substructural approach. Computational Structural Engineering: An International Journal 3, 1–7.
[31] Trinh, T.N., Koh, C.G., 2012. An improved substructural identification strategy for large structural systems. Structural Control and Health Monitoring 19, 686–700.
[32] Weng, S., Zhu, H., Xia, Y., Li, J., Tian, W., 2020. A review on dynamic substructuring methods for model updating and damage detection of large-scale structures. Advances in Structural Engineering 23, 584–600.
[33] Wu, R.T., Jahanshahi, M.R., 2020. Data fusion approaches for structural health monitoring and system identification: past, present, and future. Structural Health Monitoring 19, 552–586.
[34] Yang, T., Liu, K., Nie, G., 2021. Improved time domain substructural damage identification method on large-span spatial structure. Shock and Vibration 2021.
[35] Yuen, K.V., Huang, K., 2018. Real-time substructural identification by boundary force modeling. Structural Control and Health Monitoring 25, e2151.
[36] Yuen, K.V., Katafygiotis, L.S., 2006. Substructure identification and health monitoring using noisy response measurements only. Computer-Aided Civil and Infrastructure Engineering 21, 280–291.
[37] Zghal, M., Mevel, L., Del Moral, P., 2014. Modal parameter estimation using interacting Kalman filter. Mechanical Systems and Signal Processing 47, 139–150.
[38] Zhang, Q., Jankowski, Ł., 2017. Damage identification using structural modes based on substructure virtual distortion method. Advances in Structural Engineering 20, 257–271.
[39] Zhang, Q., Zhang, L., 2018. State estimation for stochastic time varying systems with disturbance rejection. IFAC-PapersOnLine 51, 55–59.